Office (R.N.G.), and by National Science Foundation Grant CHE 8721657 (to R.N.G.). We thank Thomas Sutto (University of Virginia) for the magnetic susceptibility measurements and Dr. P. Such (Bruker GMBH, Rheinstetten, Germany) for recording ESR spectra at liquid helium temperature.

Supplementary Material Available: Tables of atom coordinates, anisotropic thermal parameters, and mean planes for **3** and of ^1H and ^{13}C NMR data for $2/2^-$ mixtures (5 pages); tables of calculated and observed structure factors (9 pages). Ordering information is given on any current masthead page.

Semiconductor Nanocrystals Covalently Bound to Metal Surfaces with Self-Assembled Monolayers

V. L. Colvin, A. N. Goldstein, and A. P. Alivisatos*

Contribution from the Department of Chemistry, University of California, Berkeley, and Materials Sciences Division, Lawrence Berkeley Laboratory, Berkeley, California 94720.
Received March 11, 1991. Revised Manuscript Received March 2, 1992

Abstract: A method is described for attaching semiconductor nanocrystals to metal surfaces using self-assembled difunctional organic monolayers as bridge compounds. Three different techniques are presented. Two rely on the formation of self-assembled monolayers on gold and aluminum in which the exposed tail groups are thiols. When exposed to heptane solutions of cadmium-rich nanocrystals, these free thiols bind the cadmium and anchor it to the surface. The third technique attaches nanocrystals already coated with carboxylic acids to freshly cleaned aluminum. The nanocrystals, before deposition on the metals, were characterized by ultraviolet–visible spectroscopy, X-ray powder diffraction, resonance Raman scattering, transmission electron microscopy (TEM), and electron diffraction. Afterward, the nanocrystal films were characterized by resonance Raman scattering, Rutherford back scattering (RBS), contact angle measurements, and TEM. All techniques indicate the presence of quantum confined clusters on the metal surfaces with a coverage of approximately 0.5 monolayers. These samples represent the first step toward synthesis of an organized assembly of clusters as well as allow the first application of electron spectroscopies to be completed on this type of cluster. As an example of this, the first X-ray photoelectron spectra of semiconductor nanocrystals are presented.

Introduction

The ability to assemble molecules into well-defined two- and three-dimensional spatial configurations is a major goal in the field of self-assembled monolayers (SAMs).[1] Since the discovery that alkanethiols will displace practically any impurity on a gold surface[2] and will spontaneously create an ordered monolayer of high quality,[3] interest in these systems has been extensive.[4-6] Recent advances have extended SAMs beyond the prototype gold/thiol systems. Fatty acids on aluminum,[7] silanes on silicon,[8] isonitriles on platinum,[9] and rigid phosphates on metals[10] are examples. In addition to the wide choice of the substrate, the chemical functionality presented at the top of a monolayer can be controlled by replacing monofunctional alkanes with difunctional organic compounds.[11] Such assemblies can then be used to build up more complex structures in three dimensions,[12] enabling chemists to engineer complex organic structures on top of macroscopic surfaces. This specific control over the microscopic details of interfaces has allowed for diverse applications of SAMs. Metals, for example, provide the ideal support for organic compounds with large nonlinear optical behavior, and by using SAMs the molecules can be held in specific orientations with respect to the metal.[13] In other work, the ability to dictate the structural details of an interface is exploited to study processes of electron transport between an electrode surface and an active moiety bound on top of a monolayer.[14] We employ the well-developed chemistry of SAMs to attach an interesting compound, a semiconductor nanocrystal, to metal surfaces. The incorporation of clusters into the monolayers is a first step toward creating arrays of quantum dots, and the total assembly of clusters on metals represents a new kind of material with many potential uses. This new sample geometry allows us to apply photoelectron spectroscopy to semiconductor nanocrystals for the first time.

Semiconductor nanocrystals have been the subject of numerous spectroscopic investigations in recent years;[15-19] the origin of the extensive interest is that the absorption spectrum of the clusters is a strong function of their radii.[20] The clusters, in this work, cadmium sulfide, range in size from 10 to 100 Å in radius, and as their radius decreases, the electronic wave functions are confined, causing the absorption edge to shift to the blue by as much as 1 V.[20b] Despite these dramatic changes in electronic structure, only optical spectroscopies have been used to study these systems.

(1) Whitesides, G. M. *Chimia* **1990**, *44*, 310-311.
(2) Nuzzo, R. G.; Allara, D. L. *J. Am. Chem. Soc.* **1983**, *105*, 4481-4483.
(3) Porter, M. D.; Bright, T. B.; Allara, D. L.; Chidsey, C. E. D. *J. Am. Chem. Soc.* **1987**, *109*, 3559-3568.
(4) Tillman, N.; Ulman, A.; Elman, J. F. *Langmuir* **1989**, *5*, 1020-1026.
(5) Reubinstein, I.; Steinberg, S.; Tor, Y.; Shanzer, A.; Sagiv, J. *Nature* **1988**, *332*, 426-429.
(6) Bravo, B. G.; Michelhaugh, S. L.; Soriaga, M. P. *Langmuir* **1989**, *5*, 1092-1095.
(7) Allara, D. L.; Nuzzo, R. G. *Langmuir* **1985**, *1*, 45-52.
(8) (a) Maoz, R.; Sagiv, J. *Langmuir* **1987**, *3*, 1045-1051. (b) Maoz, R.; Sagiv, J. *Langmuir* **1987**, *3*, 1034-1044. (c) Wasserman, S. R.; Tao, Y.; Whitesides, G. M. *Langmuir* **1989**, *5*, 1074-1087.
(9) Hickman, J. J.; Zou, C.; Ofer, D.; Harvey, P. D.; Wrighton, M. S.; Laibinis, P. E.; Bain, C. D.; Whitesides, G. M. *J. Am. Chem. Soc.* **1989**, *111*, 7271-7272.
(10) Lee, H.; Kepley, L. J.; Hong, H.; Akhter, S.; Mallouk, T. E. *J. Phys. Chem.* **1988**, *92*, 2597-2601.
(11) (a) Bain, C. D.; Evall, J.; Whitesides, G. M. *J. Am. Chem. Soc.* **1989**, *111*, 7155-7164. (b) Pale-Grosdemange, C.; Simon, E. S.; Prime, K. L.; Whitesides, G. M. *J. Am. Chem. Soc.* **1991**, *113*, 12-20.
(12) (a) Ulman, A.; Tillman, N. *Langmuir* **1989**, *5*, 1418-1420. (b) Tillman, N.; Ulman, A.; Reuner, T. L. *Langmuir* **1989**, *5*, 101-105.
(13) Putvinski, T. M.; Schilling, M. L.; Katz, H. E.; Chidsey, C. E. D.; Mujsce, A. M.; Emerson, A. B. *Langmuir* **1990**, *6*, 1567-1571.
(14) (a) Chidsey, C. E. D. *Science* **1991**, *251*, 919-922. (b) Chidsey, C. E. D.; Bertozzi, C. R.; Putvinski, T. M.; Mujsce, A. M. *J. Am. Chem. Soc.* **1990**, *112*, 4301-4306. (c) Chidsey, C. E. D.; Loiacono, D. N. *Langmuir* **1990**, *6*, 682-691.
(15) Alivisatos, A. P.; Harris, A. L.; Levinos, N. J.; Steigerwald, M. L.; Brus, L. E. *J. Chem. Phys.* **1988**, *89*, 4001-4011.
(16) (a) Spanhel, L.; Hasse, M.; Weller, H.; Henglein, A. *J. Am. Chem. Soc.* **1987**, *109*, 5649-5655. (b) Hasse, M.; Weller, H.; Henglein, A. *J. Phys. Chem.* **1988**, *92*, 482-487. (c) Fischer, C. H.; Henglein, A. *J. Phys. Chem.* **1989**, *93*, 5578.
(17) Nosaka, Y.; Yamaguchi, K.; Miyama, H.; Hayashi, A. *Chem. Lett.* **1988**, 605.
(18) Hayes, D.; Micic, I. O.; Nenadovic, M. T.; Swayambunathan, V.; Meisel, D. *J. Phys. Chem.* **1989**, *93*, 4603.
(19) Herron, N.; Wang, Y.; Eckert, H. *J. Am. Chem. Soc.* **1990**, *112*, 1322.
(20) (a) Brus, L. E. *J. Chem. Phys.* **1984**, *80*, 4403-4409. (b) Brus, L. E. *J. Chem. Phys.* **1986**, *90*, 2555-2560.

0002-7863/92/1514-5221$03.00/0

Other experiments have not yet been performed because of limitations in the ability to control the environment of the clusters. Currently the nanocrystals can be isolated as powders for X-ray diffraction work,[21] solubilized in methanol for high-pressure studies,[22] placed in inorganic glasses or polymers for optical experiments,[23,24] and deposited by evaporation on graphite for STM imaging.[25] A serious problem with all of these media is that they do not allow the clusters to dissipate charge. As a result, the traditional probes of electronic structure and chemical environment, valence band and core level photoemission, have proved impossible to perform on nanocrystals.

In this paper we demonstrate that a solution to this problem is to uniformly disperse the clusters on a metal surface using self-assembled monolayers as a bridge. We take advantage of the extensive developments in SAMs to tailor the distance between the cluster and the metal and to tailor as well the chemical and physical properties of the substrate and bridging moiety to meet spectroscopic requirements. By providing an avenue for charge dissipation, these samples enable electron spectroscopies of the valence band density of states to be performed on nanocrystals for the first time.[26] The samples also make spectroscopy of core levels by X-ray photoemission practical. Core level XPS is redundant when applied to the atoms in the interior of the cluster, for many experiments have shown that the coordination, bond length, and compressibility of clusters are identical to those of the bulk; however, in this size range, surface atoms can make up anywhere from 20 to 60% of all the atoms. Very little is known about the bonding or structure at the nanocrystal surface, primarily because such knowledge has been irrelevant to the study of the absorption spectra, which are independent of surface derivatization. On the other hand, recent measurements of thermodynamic properties, such as melting temperature and solid–solid phase transition pressure, have shown that the chemical nature of the surface can play a dominant role in determining the cluster phase diagram. The surface structure also is a critical factor in determining the nature and intensity of particle fluorescence. XPS core level studies can ultimately be expected to provide valuable insight into the surface bonding of the clusters.

In addition to X-ray and ultraviolet photoemission experiments, the binding of the clusters to a metal surface finds application in Raman and resonance Raman scattering experiments on nanocrystals which ordinarily fluoresce strongly, in low-temperature spectroscopy of clusters, and in electrochemical studies. Since the nanocrystals can now be deposited in an asymmetric environment, intact, but in close proximity to each other, we can anticipate that the total assembly may have collective properties of considerable interest, which will be the subject of future investigations.

In the following sections the preparation of monolayers of semiconductor nanocrystals bound to both gold and aluminum surfaces is described. One technique involves building a self-assembled monolayer using alkanedithiol compounds. In comparison to other work on thiols on gold, relatively short chain alkanes are used to avoid the problem of looping. The monolayers thus formed are stable enough to withstand further chemistry on the available thiol groups. When these thiol-rich surfaces are exposed to cadmium sulfide clusters, the sulfurs form strong bonds to cadmium, anchoring the clusters to the metal (Figure 1A). An additional method involves binding the bridging group to the clusters first and then exposing the solution to the free metal (Figure 1B,C). Both techniques result in durable films of dispersed clusters, homogeneous on a micron scale with approximately 0.5-monolayer coverage. The films can be characterized by contact angle measurements, transmission electron microscopy (TEM), resonance Raman spectroscopy, and Rutherford backscattering (RBS). Ultraviolet and X-ray photoemission can be applied to the nanocrystals in this form.

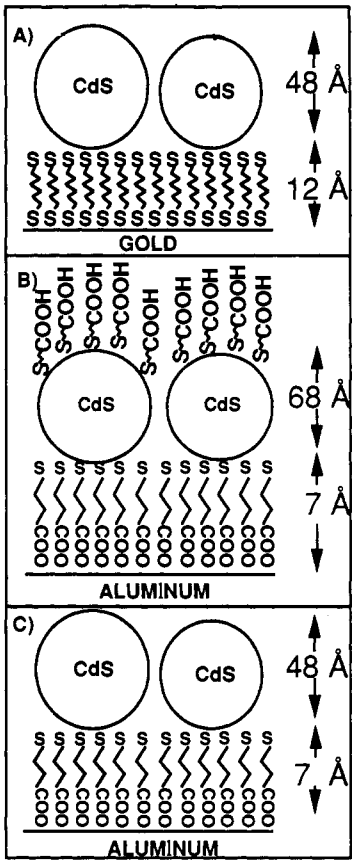

Figure 1. Schematic illustrations of cadmium sulfide nanocrystals bound to metal surfaces. (A) Cadmium sulfide from inverse micelles bound to gold via 1,6-hexanedithiol. (B) Cadmium sulfide nanocrystals synthesized in water and coated with carboxylates bound to aluminum. (C) Cadmium sulfide from inverse micelles bound to aluminum via a thioglycolic acid.

Experimental Section

I. Preparation of CdS Nanocrystals. A. Inverse Micelle Method. Cadmium sulfide clusters were prepared in inverse micelles following methods developed by Steigerwald et al.[27] and Lianos et al.[28] Two separate solutions of 500.0 mL of spectrographic grade heptane and 44.4 g of dioctyl sulfosuccinate [577-11-7], AOT, were prepared under nitrogen. $Cd(ClO_4)_2 \cdot 6H_2O$ (2.34 g) dissolved in 12.0 mL of deoxygenated, deionized water was added to one solution, while 0.36 g of $Na_2S \cdot 9H_2O$ dissolved in 12.0 mL of deoxygenated, deionized water was added to the other solution. Both solutions appeared clear and colorless after 1 h of mixing. The cadmium solution was then transferred to the sulfide via a 16-gauge double-transfer needle. The transfer process took 15 min and resulted in the formation of a clear yellow solution. At this point, 500 mL of this solution was reserved for later use, and the rest was treated with 0.45 mg of thiophenol, which binds to the surface of the clusters, causing them to come out of the micelles. The resulting powder was vacuum filtered three times and rinsed with 300 mL of petroleum ether. It was redissolved in 10 mL of pyridine and filtered again. The powder was reprecipitated into 200 mL of petroleum ether and filtered again. Refluxing of this sample was performed in 20 mL of quinoline at 240 °C for 3 h. Reprecipitation and filtering followed this, leaving a finely divided yellow powder redissolvable in pyridine.

(21) Bawendi, M. G.; Kortan, A. R.; Steigerwald, M. L.; Brus, L. E. *J. Chem. Phys.* **1989**, *91*, 7282–7290.
(22) (a) Alivisatos, A. P.; Harris, T. D.; Brus, L. E.; Jayaraman, A. *J. Chem. Phys.* **1988**, *89*, 5979–5982. (b) Hasse, M.; Alivisatos, A. P. In *Clusters and Cluster Assembled Materials*; Averback, R. S., Nelson, D. L., Bernholc, J., Eds.; MRS Symposium Proceedings; MRS Press: Pittsburgh, 1991.
(23) Ekimov, A. I.; Efros, A. L.; Shubina, T. V.; Skvortsov, A. P. *J. Lumin.* **1990**, *46*, 97–100.
(24) Liu, L.-C.; Subhash, R. *J. Appl. Phys.* **1990**, *68*, 28–32.
(25) (a) Zen, J.-M.; Fan, F. F.-R.; Guancheng, C.; Bard, A. J. *Langmuir* **1989**, *5*, 1355–1358. (b) Zhao, X. K.; Fendler, J. H. *Chem. Mater.* **1991**, *3*, 168–174. (c) Fendler et al. *Langmuir* **1991**, *7*, 1255.
(26) Colvin, V. L.; Alivisatos, A. P.; Tobin, J. G. *Phys. Rev. Lett.* **1991**, *66*, 2786.
(27) Steigerwald, M. L.; Alivisatos, A. P.; Gibson, J. M.; Harris, T. D.; Kortan, R.; Muller, A. J.; Thayer, A. M.; Duncan, T. M.; Douglass, D. C.; Brus, L. E. *J. Am. Chem. Soc.* **1988**, *110*, 3046–3050.
(28) Lianos, P.; Thomas, J. K. *Chem. Phys. Lett.* **1986**, *125*, 299–302.

B. Water-Soluble Cadmium Sulfide Clusters. Acidic colloid: A 500-mL solution of 1×10^{-3} M $CdCl_2$ was prepared, and to this was added a 500-mL solution of 1.6×10^{-3} M sodium mercaptoacetate, resulting in a turbid blue solution. The pH was lowered to 3.35 with HCl, producing a colorless solution. Na_2S (150 mL, 1×10^{-2} M) was then injected to the quickly stirring solution. This preparation gave particles with an absorption maximum at 460 nm. Crystallites with absorption maxima as low as 360 nm could be obtained by reducing concentrations.

Basic colloid: $CdCl_2$ (1 L, 1×10^{-3} M) was titrated with mercaptoacetic acid to pH 2.8, resulting in a turbid blue solution, as above. Concentrated NaOH was then added dropwise until the pH was greater than 8.5 and the solution was again colorless. While the solution was quickly stirred, 110 mL of 1×10^{-2} M Na_2S was added. Particle sizes with absorption maxima between 360 and 410 nm were produced by varying the final pH of the thiol titration.

The colloids from both preparations were reduced by rotary evaporation to a redissolvable powder, which contained NaCl as a reaction byproduct. Dialysis against a dilute solution of mercaptoacetic acid was necessary to remove the salt while maintaining the solubility of the colloids. Solutions of redissolved crystallites were stable in the dark for months. All reactions were conducted in room light using deionized, distilled water. The colloids can be grown by heating to 90 °C in the presence of 0.5 mL of the thiol.

II. Attachment of Clusters to Metals. A. Preparation of Metal Substrates. Some of the metal layers used in these experiments were prepared by vapor deposition of gold or aluminum onto glass slides. The vapor deposition was performed at 10^{-7} Torr in a bell jar; evaporations usually took 10 min and resulted in films with an average thickness of 1000 Å. The thickness was determined by a quartz crystal microbalance inside the bell jar. Adhesion of the gold films to the glass slide was insured by use of a "molecular glue", (3-mercaptopropyl)trimethoxysilane. The details of this procedure have been described by Majda and co-workers.[29] Reproducible high-quality films were obtained only when the glass slides were cleaned prior to treatment by immersion in 1:4 reagent grade 30% H_2O_2/concentrated H_2SO_4 (piranha) at 70 °C for 10 min. **CAUTION**: "Piranha" solutions react violently with many organic materials and should be handled with extreme care!

In addition to the evaporated films, metal blocks were also used as substrates to facilitate mounting of the samples to spectrometers and cryostats. For aluminum samples, solid aluminum was machined into an appropriate size with a satin finish. For a gold substrate, a 1-μm-thick layer of gold was electroplated onto the aluminum blocks; in this procedure significant etching of the aluminum produced a much smoother surface with a mirror finish. These block samples, although ideal for low-temperature applications and photoemission, were more rough, and coverages for some of the samples, especially the water-soluble CdS clusters on aluminum, were lower.

B. Preparation of Dithiol Monolayers on Gold. Self-assembled monolayers were prepared by immersing gold substrates in dilute solutions of hexanedithiol following established methods.[11,30] The substrates were plasma etched before use for 10 min at 200 mTorr in N_2 atmosphere. Contact angles after such etching were less than 10°, indicating a clean surface. The samples were placed in a 5 mM ethanolic solution of dithiol for 8–12 h. Gold substrates were coated with 1,6-hexanedithiol (Figure 1A). After immersion the samples were removed from solution, rinsed with ethanol for 30 s, and then blown dry with argon. Contact angle measurements were performed at this time. Different lengths of dithiol were used with little success; propanedithiol monolayers on gold gave low contact angles, and XPS showed little evidence of sulfur, while octanedithiol on gold gave high contact angles and resulted in low nanocrystal coverages. All thiols were purchased from Aldrich; 1,6-hexanedithiol was 97% pure, and mercaptoacetic acid was 95% pure. Under ambient conditions, the dithiols will interconvert to disulfides; a disulfide impurity has little impact on the films since thiol groups are 100-fold more efficient at binding to gold.[31]

C. Preparation of Thiol Monolayers on Aluminum. Aluminum was treated with mercaptoacetic acid to make its surface thiol rich (Figure 1B), following methods developed by Nuzzo et al.[7] Although freshly evaporated aluminum has a low contact angle, plasma etching was performed on the substrates prior to immersion. Etched substrates were placed immediately in solutions of 5 mM mercaptoacetic acid dissolved in ethanol and were allowed to sit for 12 h. The substrates were removed, rinsed with ethanol for 30 s, and blown dry with argon. Samples could be stored in a desiccator prior to coating with nanocrystals.

D. Preparation of Cluster Monolayers. Both the aluminum and gold substrates were prepared such that their surfaces contained free thiols. These SAMs were then exposed to solutions of cadmium sulfide clusters in micelles. These solutions contain heptane, AOT, and clusters. Exposure was completed in much the same way as for the original monolayers: the sulfur-rich SAMs were immersed in solutions of heptane containing the inverse micelles. The heptane solutions were used undiluted and hence had an approximate concentration of 2.70 g of cadmium sulfide/L. Typical immersion time was 12 h, and afterward the samples were rinsed with heptane for 30 s and then blown dry with argon. The treatment afterward was identical to the preparation of the SAMs. The films were indefinitely stable.

An additional method which bypasses the use of a preliminary monolayer was also developed. In this case, nanocrystals prepared with carboxylate-rich surfaces were exposed to freshly etched aluminum. The dialyzed powders were dissolved in nanopure water with 18-MΩ resistivity in concentrations of 4 mg/mL. The aluminum substrates were immersed in the water solutions for 24–48 h. Treatment after immersion included a 30-s water rinse followed by drying with argon gas.

III. Characterization of Samples. A. Ultraviolet–Visible Spectroscopy. Ultraviolet–visible spectroscopy was performed on a Hewlett-Packard 8405A diode array spectrometer. The resolution of the machine was 2 nm, and typical optical densities at the peak of the first excitonic feature were 0.2–1. Cadmium sulfide nanocrystals were dissolved in either water or heptane, both of which do not contribute any significant background in the region of interest, 300–500 nm. The size of the crystallites was determined using the relationship between the absorption peak of the first excited state of the crystallite and size, as calculated by the tight-binding method of Lippens and Lannoo[32] which includes a correction for Coulombic attraction between the electron and the hole.

B. X-ray Powder Diffraction. X-ray powder diffraction was performed on the isolated cadmium sulfide powders on a Siemens PDA 5000 diffractometer equipped with a Cu Kα tube and a scintillation counter. Instrument resolution (0.05° 2θ) was far narrower than the observed peak widths. Typical integration times lasted 4 h.

C. Transmission Electron Microscopy and Electron Diffraction. Micrographs were obtained at the National Center for Electron Microscopy at the Lawrence Berkeley Laboratory, on a JEOL 200 CX microscope operating at 200 kV, with spatial resolution of 2.2 Å. Clusters were deposited on plasma-etched amorphous carbon substrates supported on 600-mesh copper grids. Nanocrystals were deposited from solutions by evaporation of the solvent. Thin aluminum films (200 Å thick) with colloids bound to them were floated free of a salt substrate and supported on a 600-mesh copper grid. These films were polycrystalline, with a grain size of several unit cells. Aluminum platelets of ~400 Å composed of randomly oriented 100-Å domains were either embedded in or lying on the surface. Selected area electron diffraction patterns, using a 0.2-μm^2 aperture for Figure 6 and a 0.03-μm^2 aperture for Figure 16, were recorded on film, and the negatives were digitized using a 2048-element CCD camera.

D. Contact Angle. Contact angle measurements were performed on a Rame-Hart Model 100 contact angle goniometer using deionized water at ambient humidity. Advancing contact angles were measured three times at different places on the films. The metal block samples were not appropriate for contact angle measurements due to their surface roughness.

E. Resonance Raman Spectroscopy. Resonance Raman spectroscopy was performed with a tunable dye laser as the excitation source from 400 to 457 nm and with lines from an argon ion laser for wavelengths between 457 and 514.5 nm. A SPEX triple monochromator with a final stage grating blazed at 500 nm and with 1800 grooves/mm was used to isolate the inelastically scattered light. A Photometrics liquid nitrogen cooled CCD camera with a PM 512 chip recorded the spectrum. The average spot size was on the order of 5 μm, and typical scans took 20 min with 5–20-mW incident power. Some cluster monolayers showed a decrease in signal after being exposed to the laser for over 1 h. This photochemical degradation is also observed with nanocrystals in solution and is not unique to the metal films.[33] At low temperatures and in vacuum this did not occur. Resonance Raman excitation profiles were obtained at ambient temperature. Cross sections were determined relative to a quartz standard by sample substitution.

F. Photoemission Spectroscopy. X-ray photoemission spectroscopy was performed on a Perkin-Elmer ESCA 5400 spectrometer equipped with a hemispherical energy analyzer. The supply was operated at 400 W and 15 V with the Mg Kα monochromatized X-ray source. The resolution of the spectrometer was 0.8 V. There was no evidence of film

(29) Goss, C. A.; Charych, D. H.; Majda, M. Submitted for publication in *Anal. Notes*.
(30) Bain, C. D.; Troughton, E. B.; Tao, Y.; Evall, J.; Whitesides, G. M.; Nuzzo, R. G. *J. Am. Chem. Soc.* **1989**, *111*, 321–335.
(31) Bain, C. D.; Biebuycky, H. A.; Whitesides, G. M. *Langmuir* **1989**, *5*, 723–727.
(32) Lippens, P. E.; Lannoo, M. *Phys. Rev. B* **1989**, *39*, 10935.
(33) Henglein, A. *Top. Curr. Chem.* **1988**, *143*, 113–180.

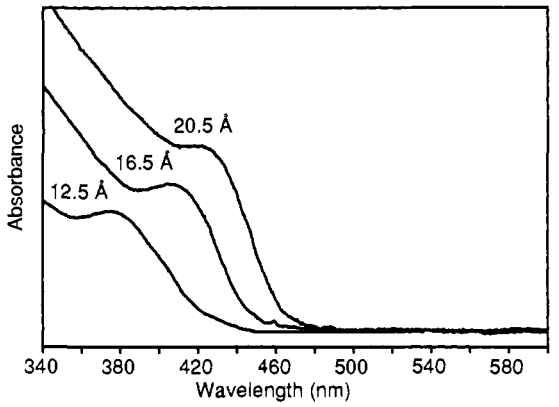

Figure 2. Ultraviolet–visible spectra of CdS clusters in heptane/micelle mixtures. The radii listed were determined by the absorption maximum and ref 32.

degradation over time, and scans lasted usually 1 h. Base pressure in the chamber was 5×10^{-8} to 1×10^{-9} Torr. At these base pressures, in 1 min 50% of the sample surface will have suffered a collision with a gas molecule. Given that the most common UHV (ultrahigh vacuum) contaminant gases are CO and water, both of which have fairly high sticking coefficients, the XPS carbon and oxygen core level intensities are not easily analyzed. It was necessary to ground the films in order to prevent charging. The gold samples provided the Au 4f peaks at 83.8 eV as calibration. UPS (ultraviolet photoelectron spectroscopy) measurements were performed at the University of Wisconsin Synchrotron Radiation Center on the 4-m normal incidence monochromator beam line. The spectrometer used a multichannel analyzer with a resolution of 0.2 eV.

G. Rutherford Backscattering. RBS was performed on the films at the Lawrence Berkeley National Laboratory RBS facility. Only aluminum samples could be tested as the gold RBS signal interferes with the detection of cadmium and sulfur.

Results

Due to the novel nature of the clusters, the initial thiol monolayers, and the cluster–metal samples, many different characterization techniques were used at all stages of the process. The determination of the size and crystallinity of the clusters before binding to metals is necessary to assess any changes in the clusters upon deposition. Certain standard characterization techniques for nanocrystals, such as X-ray diffraction and ultraviolet–visible spectroscopy, can only be performed on monolayer samples with great difficulty and were completed on samples before attachment. The thiol monolayers themselves on both gold and aluminum, although synthesized by standard techniques, were studied by XPS in order to obtain information concerning the amount and chemical state of the monolayer sulfur. Finally, the characterization of the combined cluster–metal systems involved many techniques in order to determine both the coverage and the morphology of clusters on the surface.

Characterization of Clusters before Deposition. Solution-phase studies of the clusters before exposure to metals provide information about the size and crystallinity of the samples. Size is most easily found from the ultraviolet–visible spectra of the clusters (Figure 2). The position of the absorption edge depends on size because of quantum confinement. This relationship was made quantitative by tight-binding calculations[32] of the energy of the first electronic excited state of the clusters and hence provides the basis for sizing. The absorption spectra also give an estimate of the size distribution from the sharpness of the absorption feature.[15] For the samples used in these experiments, typical size distributions are ±5% on the diameter.

The crystallinity of these systems before deposition on a metal can be studied by both X-ray diffraction and selected area electron diffraction. X-ray diffraction on powders isolated from these solutions indicates the particles to be crystalline and of the zinc blende lattice structure (Figure 3). The finite size of the crystallite causes a broadening of the diffraction lines which can be related to size by the Debye–Scherrer formula, and thus Gaussian fits to the diffraction peaks provide a measure of cluster size. In addition, the smaller clusters show a lattice contraction due to

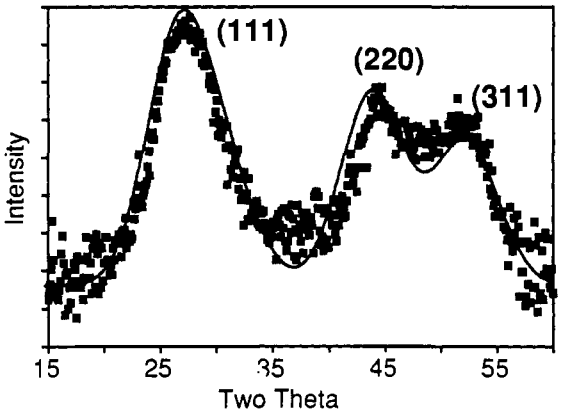

Figure 3. X-ray diffraction spectra of a CdS cluster powder. Typical X-ray diffraction pattern from zinc blende 14.5-Å-radius CdS clusters isolated from micelle solutions. The solid line represents a fit to the data using the Debye–Scherrer formula.

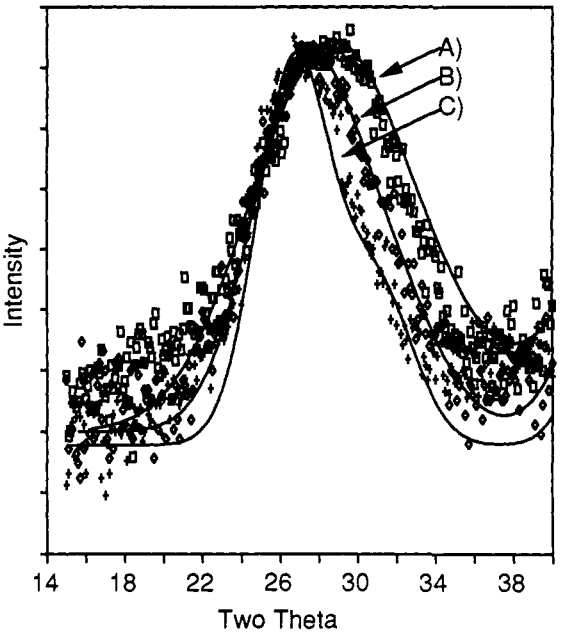

Figure 4. An expanded view of the (111) Cu Kα X-ray diffraction peak for three different sizes of CdS clusters isolated from micelle solutions. The Debye–Scherrer fits were corrected for both the finite size and lattice contraction in small particles: (A) 10-Å-radius CdS clusters with 3.22-Å spacing (squares); (B) 14.5-Å-radius CdS clusters with 3.28-Å spacing (diamonds); (C) 20-Å-radius CdS clusters with 3.36-Å spacing (pluses).

surface tension (Figure 4).[34] Direct imaging of the lattice planes by transmission electron microscopy (TEM) shows crystalline spherical particles (Figure 5). Many randomly oriented particles provide an electron diffraction pattern which confirms that the particles are zinc blende cadmium sulfide (Figure 6). As in X-ray diffraction, finite domain size leads to a broadening of the diffraction lines which can be related to size using the Debye–Scherrer formula. Such measurements of size are in good agreement with sizes obtained by counting and sizing many imaged clusters.

Characterization of Self-Assembled Monolayers. Self-assembled monolayers before exposure to solutions of CdS were studied by contact angle measurements and XPS. On the gold substrates, contact angle measurements of the hexanedithiol layers gave contact angles of 40–50°; this value lies in between values reported for mercapto alcohols and long-chain hydrocarbons on gold,[11] as expected since thiol groups have intermediate polarity. Contact angles on the aluminum samples were not informative since they were always 5°. XPS on both aluminum and gold samples showed

(34) Goldstein, A. N.; Alivisatos, A. P. Submitted for publication.

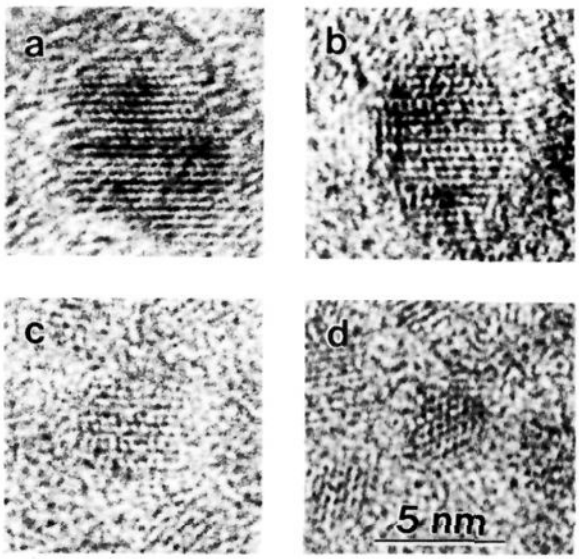

Figure 5. TEM images of CdS clusters of different size reveal lattice planes. The bar in panel d corresponds to 50 Å, and the magnification is the same in all four panels. A statistically large enough sample of such images provides a basis for sizing.

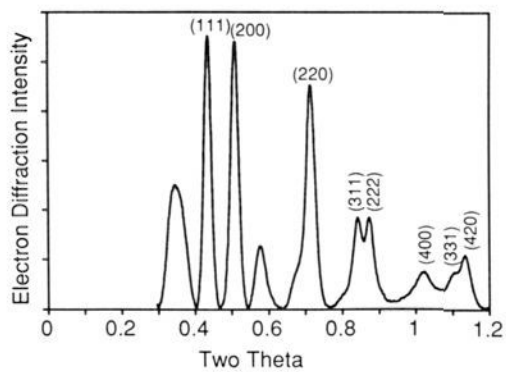

Figure 6. The selected area electron diffraction pattern of 14.5-Å-radius CdS particles reveals eight diffraction rings. The Debye–Scherrer fit gives the same size as the X-ray diffraction data. The two unlabeled peaks correspond to the amorphous carbon substrate.

evidence of sulfur (Figures 7A and 8A,B) on the surface. The position of the core at 168 eV is consistent with the presence of sulfur in the monolayer, while the lower peak near 162 eV is consistent with a metal sulfide species. The value of the sulfur peak at 168 eV is representative of a sulfate or sulfonic acid moiety rather than an organic thiol. It is possible that the monolayers suffered beam-induced damages from the X-ray source, which could cause an oxidation of the sulfur thiols.[35] Additional peaks, especially from carbon and oxygen, dominated the spectrum since the samples were not cleaned in vacuum. Given the 100-Å escape depth of the electrons in XPS, the gold and aluminum core levels from the metal were easily visible. The gold 4f core was at 83.8 eV, in agreement with literature, indicating that these samples were not charging.

Characterization of Clusters Bound to Metals. After immersion in the cadmium sulfide solutions, the metal/cluster systems were characterized by contact angle, resonance Raman, XPS, RBS, and TEM. A successful coat was indicated by a contact angle between 15° and 25°. The metals exposed to the cadmium sulfide solutions appeared the same to the eye as plain metal surfaces; in the case of binding carboxylate-coated clusters to aluminum,

(35) Such a problem has been observed during specular X-ray reflection on alkylsiloxane monolayers (see ref 33), although beam intensities were at least 2 orders of magnitude higher. Some researchers have alluded to this problem with thiol layers on gold, but no description of the actual effects of beam damage has been described for these systems.

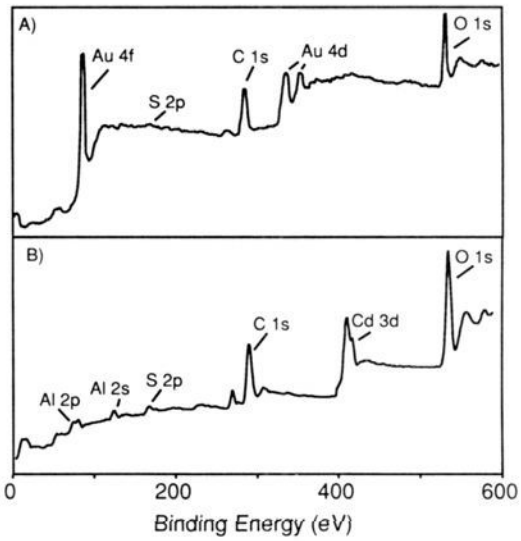

Figure 7. (A) XPS scan of 0–500-eV binding energy for gold with just a hexanedithiol layer. Carbon and oxygen are the dominant peaks given that the sample was not cleaned in vacuum. (B) XPS scan of an aluminum sample treated with mercaptoacetic acid and then 25-Å-radius CdS clusters (Figure 1B).

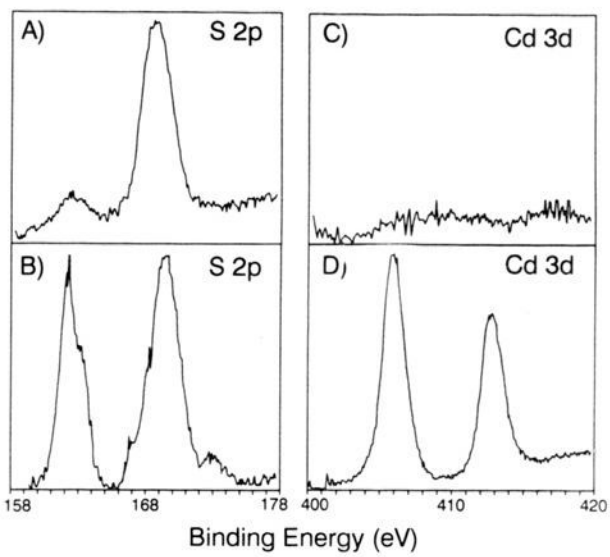

Figure 8. XPS data of cadmium 3d and sulfur 2p core levels. (A) Sulfur 2p from hexanedithiol bonded to gold. The feature at 168 eV is an oxidized form of sulfur, and the 162-eV peak is the metal sulfide. (B) Sulfur 2p from 20-Å-radius CdS on gold. (C) Cadmium 3d peak of the hexanedithiol sample indicating no cadmium. (D) After deposition of CdS, a Cd 3d doublet is observed. The ratio of cadmium to sulfur is roughly 3:4.

corrosion would sometimes occur. This could be avoided by keeping the pH near 7.

X-ray photoemission studies of the nanocrystal monolayers indicated the presence of both cadmium and sulfur on the metal surface (Figures 8B,D) in a roughly 3:4 ratio. A full survey scan (Figure 7B) shows the presence of carbon and oxygen as well as cadmium, sulfur, and the underlying metal. A small sodium peak, a counterion in the production of the clusters, has also been assigned. Although the relative cross section of sulfur is small in comparison to that of other elements, the sulfur peaks are particularly sensitive to the chemical environment. The lower energy peak at 163.2 eV is indicative of a metal sulfide, while the peak at 168.8 eV has been assigned to a more oxidized form of sulfur.[36-38] Such a result is in agreement with studies of bulk

(36) (a) Lichtensteiger, M.; Webb, C.; Lagowski, J. *Surf. Sci.* **1980**, *97*, L375–L379. (b) Lichtensteiger, M.; Webb, C. *J. Appl. Phys.* **1983**, 2127.

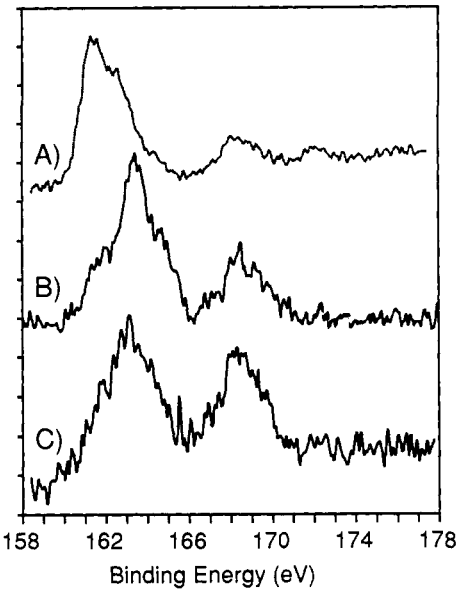

Figure 9. Comparison of the sulfur peaks of CdS bound to aluminum as a function of cluster size: (A) 32-Å-radius CdS; (B) 18-Å-radius CdS; (C) 14-Å-radius CdS. The (aluminum bound) sulfide peak increases in intensity relative to the sulfate in larger nanocrystals. Gold samples also show similar trends, but the results are clouded by the preexisting 168.5-eV sulfur peak from the monolayer (see Figure 8A and ref 36).

cadmium sulfide which indicate the presence of a 168.8-eV sulfate peak even under relatively clean UHV conditions.[35-37] Figure 9 shows a comparison of the sulfur 2p core peaks for three different sizes of CdS; as a sample becomes smaller, the ratio of the low-field sulfur to the high-field sulfur decreases. This result suggests that the sulfur occurring at 168.8 eV originates from a surface sulfur species, as observed in the bulk studies.[39] In addition, the low-field sulfur from 161 to 165 eV appears to shift to higher binding energies. This peak is actually two peaks, one corresponding to a metal sulfide at 162 eV and the other at 164 eV, an organic thiol at the particle surface.[40] For smaller sizes, and hence larger surface to volume ratios, the organic thiol contribution increases, making the total peak appear to shift.

Although XPS measurements show the presence of both cadmium and sulfur, they do not directly distinguish between atoms and clusters since they access atomic cores which are only indirectly sensitive to cluster size. Measurements of the bonding electrons, using ultraviolet photoemission, provide a more direct test for the presence of clusters. Figure 10 shows the valence band photoemission spectra taken with synchrotron radiation. The peak at 12 eV is a shallow 4d cadmium core, while the broad peak centered at 6 eV is the valence band. The general shape and position of the valence band is in agreement with measurements of bulk cadmium sulfide,[41] except that the exact position of the threshold is a function of cluster size. This shift with size can be explained in terms of existing theories of quantum confinement and dielectric solvation[42] and is the subject of a separate investigation.[26]

Resonance Raman measurements confirm the presence of quantum-confined clusters on both gold and aluminum surfaces.

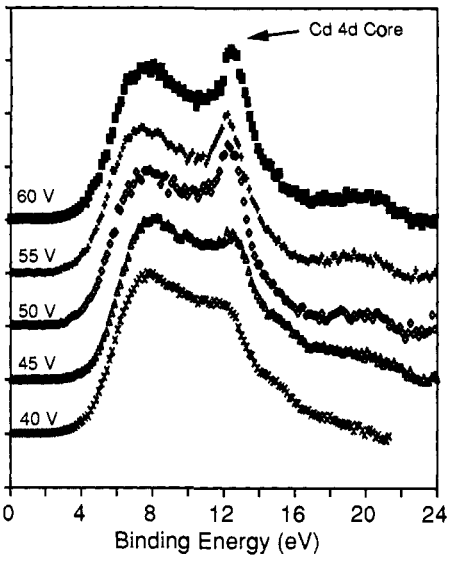

Figure 10. UPS spectra of 36-Å-radius CdS bound to aluminum as in Figure 1C. As the exciting photon energy is increased, the cross section of the Cd 4d orbital is enhanced.

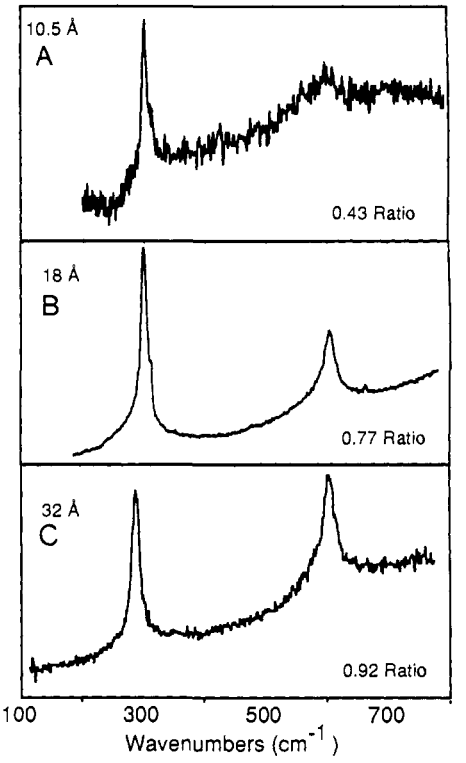

Figure 11. Resonance Raman spectra from CdS clusters on metals as a function of size. The peak at 300 cm^{-1} is the first longitudinal optical phonon (1LO) while the peak at 600 cm^{-1} is the overtone (2LO): (A) 10.5-Å-radius CdS; (B) 18-Å-radius CdS; (C) 32-Å-radius CdS. As the clusters become larger, the ratio of the 1LO to the 2LO increases.

Figure 11 shows resonance Raman spectra from metal films covered with CdS. As observed for powders of nanocrystalline CdS,[43] the second longitudinal optical mode (2LO) at 600 cm^{-1} is smaller than the first longitudinal optical mode (1LO) at 300 cm^{-1}. In addition, the ratio of the 1LO to the 2LO is a smooth function of size as shown in Figure 11. This data is consistent with clusters of cadmium sulfide,[44] not bulk cadmium sulfide which has a larger 600-cm^{-1} mode, relative to the fundamental.[45] The

(37) (a) Amalnerkar, D. P.; Badrinarayanan, S.; Date, S. K.; Sinha, A. P. B. *Appl. Phys. Lett.* **41**, 270–271. (b) Amalnerkar, D. P.; Badrinarayanan, S.; Date, S. K.; Sinha, A. P. B. *J. Appl. Phys.* **54**, 2881–2882.

(38) Marychurch, M.; Morris, G. C. *Surf. Sci.* **1985**, L54, L251–L254.

(39) Clusters prepared on aluminum without the presence of a thiol monolayer possess a 168.8-eV peak, indicating that the peak arises not from an oxidized thiol monolayer but from the clusters. However, on the pretreated samples, the underlying sulfur monolayer may contribute to this feature. Further experiments using synchrotron radiation to tune electron escape depth are underway in order to separate the contributions from the monolayer and the cluster.

(40) Nuzzo, R. G.; Zegarski, B. R.; Dubois, L. H. *J. Am. Chem. Soc.* **1987**, *109*, 733–740.

(41) Ley, L., et al. *Phys. Rev. B* **1974**, *9*, 600–623.

(42) Brus, L. E. *J. Chem. Phys.* **1983**, *79*, 5566–5571.

(43) Alivisatos, A. P.; Harris, T. D.; Carroll, P. J.; Steigerwald, M. L.; Brus, L. E. *J. Chem. Phys.* **1989**, 3463–3467.

(44) Shiang, J. J.; Goldstein, A. N.; Alivisatos, A. P. *J. Chem. Phys.* **1990**, *92*, 3232–3233.

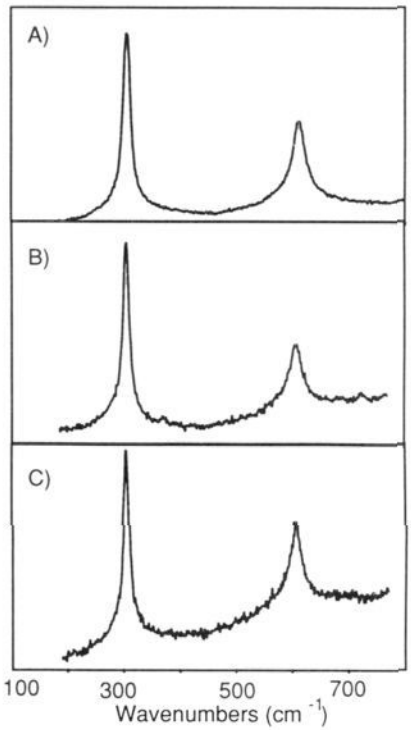

Figure 12. Resonance Raman spectra from three different cluster-on-metal samples: (A) 35-Å-radius CdS clusters bound to aluminum from water solution; (B) 36-Å-radius CdS clusters bound to aluminum from inverse micelles via thioglycolate; (C) 36-Å-radius CdS bound to gold via hexanedithiol. The metal and the bridging moiety have no effect on the spectra.

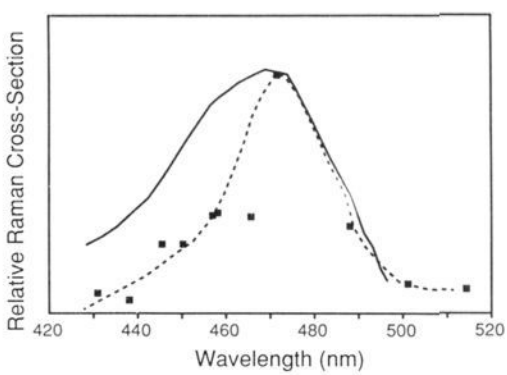

Figure 13. Excitation profile of carboxylate-coated CdS on aluminum (Figure 1C) (dashed line), and the same particle in solution (solid line). The width of the peak appears to narrow for clusters bound to metals, but low-temperature measurements are needed to confirm this conclusion.

intensity of the resonance Raman spectra did not change from spot to spot on the samples, when the laser beam was focused to approximately 5-μm diameter.

Resonance Raman excitation spectra (Figure 12) were obtained by tuning the exciting laser wavelength; such spectra give information about the size distribution of the clusters, since the Raman cross section peaks at the same place as the ultraviolet–visible spectrum. The excitation profile of clusters on aluminum (Figure 13) shows that the size of the clusters is the same on the metal surface as in the original solution. Another important result is that the width of the profile is about the same, indicating that the size distribution does not change significantly upon deposition. Finally, the magnitude of the resonance Raman signal is smaller than that observed for CdS powders or CdS in pyridine.

While resonance Raman identified the presence of quantum-confined clusters, Rutherford backscattering (RBS) experiments

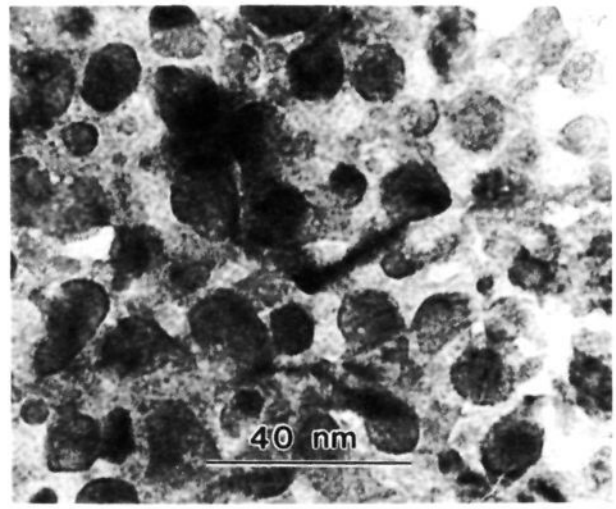

Figure 14. Transmission electron micrograph of CdS clusters on aluminum (Figure 1C). The light mottled background is from the polycrystalline aluminum film while the darker spots are the CdS clusters. The average radius of CdS clusters in this sample is 35 Å.

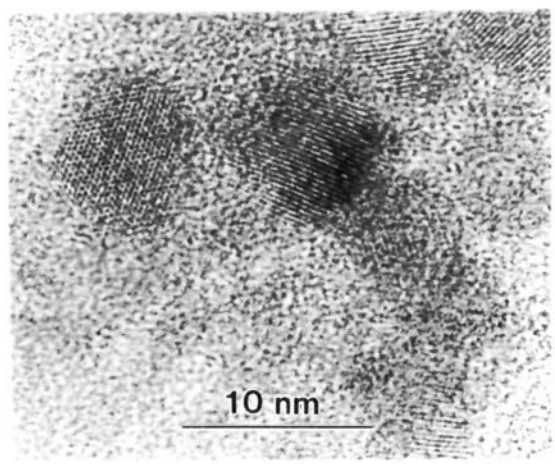

Figure 15. Transmission electron micrograph of single particles of CdS on aluminum. This micrograph shows several clusters magnified so that the lattice planes are visible.

gave a quantitative measure of the number of cadmium and sulfur atoms at the metal surface and hence the coverage of clusters. Only the aluminum samples were amenable to this technique as the gold, being of heavy mass, interferes with other peaks. Average coverages were measured in terms of cadmium or sulfur atoms/cm^2. These numbers could be converted into cluster coverages using the radius of the clusters as determined from ultaviolet–visible spectroscopy, and assuming one monolayer of clusters to be a close-packed layer of spheres. A typical value for cadmium atoms/cm^2 was 3×10^{15} atoms/cm^2 while that for sulfur atoms was 2×10^{15} atoms/cm^2, which for 20-Å-radius particles corresponds to a coverage of 0.4 atoms/cm^2. RBS depth profiling measurements also indicated that the cadmium and sulfur atoms were on top of the aluminum, as expected.

A more direct way to probe surface morphology is to use TEM. By using thin (less than 200 Å) films of aluminum for a substrate, TEM images of the actual surface can be obtained.[46] Figure 14 shows a large section of a surface of an aluminum sample which was treated with carboxylate-coated clusters. In large areas the clusters are dispersing homogeneously on the surface; however, blank regions of the film were also imaged. A closer image of these clusters, revealing lattice planes, is shown in Figure 15. In order to verify that the dark spots were actually crystalline CdS clusters, selected area electron diffraction was performed on the

(45) Klein, M. L.; Porto, S. P. S. *Phys. Rev. Lett.* **1969**, *22*, 782–787.

(46) Strong, L.; Whitesides, G. M. *Langmuir* **1988**, *4*, 546–558.

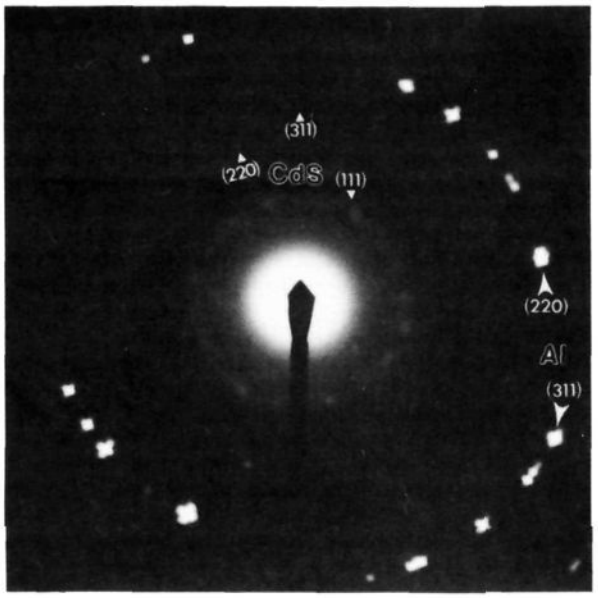

Figure 16. Selected area electron diffraction taken of a region of aluminum/CdS surface. CdS diffraction peaks as well as aluminum peaks are clearly visible.

samples. The results are shown in Figure 16; both CdS diffraction patterns and aluminum diffraction patterns are observed.

Discussion

The evidence from a variety of characterization techniques indicates that CdS clusters can be bound to metal surfaces using self-assembled monolayers. The nanocrystals are deposited intact, without fusion or aggregation, but at relatively high coverage. In this form, electron spectroscopies can be performed on the clusters, without any charging. The samples are durable, lasting for months in air without degradation. The general technique of attaching clusters to metals via an organic bridge is versatile; it is successful whether the bridge group is first attached to the metal or to the nanocrystal. These samples have already proven useful in spectroscopic investigations of semiconductor nanocrystals.

Clusters Are Deposited Intact, without Fusion or Aggregation. XPS data indicates the presence of atomic sulfur and cadmium on treated surfaces (Figures 7 and 8). Resonance Raman spectroscopy shows that samples prepared by a variety of techniques have modes at 300 and 600 cm^{-1}, in agreement with measurements of bulk cadmium sulfide and cadmium sulfide nanocrystals in solution (Figures 11, 12, and 17). Resonance Raman data also indicate that the clusters do not fuse on the metal surfaces. Previous work has shown that quantum-confined clusters, while having spectra similar to that of bulk CdS, have different overtone ratios, and that the ratio of the fundamental to the overtone increases smoothly with decreasing size.[42,43] This trend is observed in the metal-bound nanocrystal samples (Figure 11), as particles of different sizes deposited on metal surfaces show an increase in the ratio of the 1LO to the 2LO with decreasing size. Finally, TEM imaging of thin films of CdS-treated aluminum clearly shows the presence of small crystalline clusters whose electron diffraction pattern is consistent with small zinc blende CdS clusters (Figures 14 and 15).

An important parameter in the study of clusters is the size distribution. It is possible that kinetic or thermodynamic factors could favor the binding of one size over another, resulting in a narrower size distribution for bound clusters, compared to the distribution in the solution phase. To investigate this possibility, we measured size distributions before and after deposition using Raman excitation spectra (Figure 13). Both samples peak at the same wavelength. Within the error of the measurements, the CdS clusters bound to metals appear to have a narrower distribution of sizes (i.e., their excitation width is smaller) than the parent solution. In order to resolve this unambiguously, additional 1.6 K measurements are now in progress. Low temperature is a necessary condition because the width of the homogeneous optical spectrum is a strong function of temperature and is comparable to the inhomogeneous width at room temperature. While the size distribution of the clusters on metals is of great interest, the most important result is that the position of the resonance Raman excitation peaks in solution and on the metal coincides with the measured absorption peak for these 35-Å-radius nanocrystals. This coincidence of the resonance Raman excitation spectrum peak with the quantum-confined solution-phase optical absorption spectrum provides additional conformation that the particles are deposited intact without aggregation.

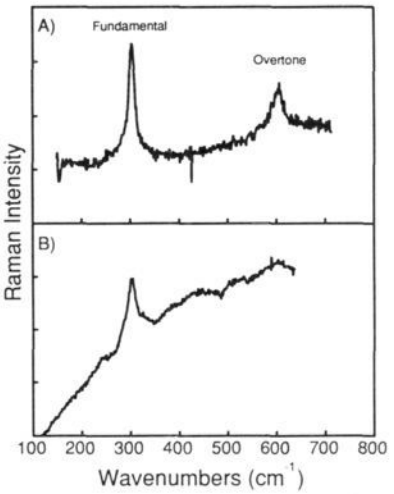

Figure 17. (A) Resonance Raman spectra from CdS clusters on aluminum. (B) Resonance Raman spectra of CdS clusters in solution. The broad sloping background from fluorescence disappears when clusters are bound to metals.

The efficiency of the resonance Raman process for clusters falls rapidly with decreasing size,[43] making detection of a monolayer difficult for smaller clusters (Figure 11A). For this reason, X-ray photoemission (XPS) is complementary to the resonance Raman characterization. The signature of any size cadmium sulfide cluster on the surface is the presence of a metal sulfide peak at 163.2 eV in conjunction with the cadmium $3d_{5/2}$ core at 405.8 eV (Figure 8B,D). Sulfurs from the cluster surface give a peak at 168 eV. As expected from surface to volume arguments, the relative amounts of each of these changes smoothly with cluster size (Figure 9). In addition, smaller clusters of CdS allow more photoelectrons to escape from the metal given that the escape depth at these energies is 100 Å; hence the cadmium to metal substrate ratio is smaller when smaller particles are bound to the metal.

XPS Allows Identification of Surface Sulfur Species. The sulfur peak observed at 168.8 eV (Figure 9) can be assigned to a surface sulfate group. Extensive studies of bulk cadmium sulfide by XPS have shown that sulfur at the surface of bulk single crystal cadmium sulfide,[35,37] as well as sulfur in polycrystalline thin film cadmium sulfide,[36] has a signature XPS peak at 169.0 eV. Several studies have conclusively assigned this peak to a sulfate moiety, SO_4^{2-}, and have shown that water, not oxygen or light, is responsible for the oxidation reaction.[35-37] Since all preparations of the particles used in these experiments were in bulk water, or in water pools of inverse micelles, it is likely that the surface and subsurface sulfurs were oxidized before they were bound to the metal surface. The propensity of bulk cadmium sulfide to oxidize has long been observed by electrochemists,[47] and these results confirm that the process occurs in clusters of cadmium sulfide as well. This observation will have far-reaching implications for the synthesis of clusters, as well as the understanding of their luminescence, which is known to be controlled by surface defects. Not all of the surface sulfur is in an oxidized form, since there

(47) Meissner, D.; Benndorf, C.; Memming, R. *Appl. Surf. Sci.* **1987**, 423-426. Meissner, D.; Memming, R.; Kastening, B. *J. Phys. Chem.* **1988**, *92*, 3476-3483.

is a peak at 164 eV which grows larger with smaller particle size. The assignment of this feature to an organic sulfur is consistent with photoemission studies of thiols on single crystal gold which indicate the 164-eV peak to be from an organic sulfur.[39] Its larger contribution in smaller sizes of CdS, in which over half the atoms are on the surface, indicates that it originates from the surface of the cluster.

Coverage Is Half a "Monolayer". Rutherford backscattering measurements yield a coverage near half a monolayer. This method averages over micrometers, and sampling over different regions of the samples shows that there is little variation in the coverage. Direct transmission electron microscopy measurement of the coverage confirms most aspects of these results. TEM is impossible to perform on the micrometer-thick metal surfaces on which the clusters are normally deposited, since the metal attenuates the diffracting electron beam. Following Strong and Whitesides[45] this difficulty was overcome by attaching the nanocrystals to a very thin (200-Å or less) film of aluminum, which was floated onto a Cu TEM grid. The images obtained are shown in Figure 14. The clusters in these photos appear well-dispersed over a large area of the substrate. They are very closely packed, and the observed coverage is commensurate with that measured by RBS. One characteristic of the TEM photos is that not all of the aluminum surface is coated. There are some areas which are quite bare. The typical length of a "patch" was 0.5–1 μm; the large-scale patches in this sample were surprising, given the high degree of uniformity observed in the Raman and RBS measurements. The most likely reason for this discrepancy is the lack of structural integrity in the thin Al films; buckling or folds would prevent binding of the particles in those areas, leading to the large-scale patchiness. Hence, Figure 14 is likely to be representative of the surface in properly formed monolayers. TEM results on the aluminum surfaces indicate that the clusters bind to the surface without clumping or stacking to form homogeneous layers of 0.5–1 atoms/cm^2 coverage. Given the agreement of all other characterization data of the three kinds of samples, it is likely that this conclusion also holds for the other two sample types (Figures 1A,B).

Length of the Bridging Moiety. A number of factors governed the choice of chain length for the dithiols. The alkane chain needs to be short enough that looping of the bifunctional bridging moiety does not occur. The metal must be close enough to dissipate charge during photoemission and other electron spectroscopy experiments, but not so close as to alter the energies and densities of the cluster electronic states. Our choice of 7–12-Å chain lengths balances these various factors.

Dithiols and thiol acids with short chains were used to build the initial monolayers. This point deserves comment, since most investigators have used much longer chain hydrocarbons in the preparation of monolayers. Previous studies of SAMs have determined that longer chain molecules, C_{10} or longer, are necessary for the formation of crystalline monolayers,[2,7] because it is the lateral interactions between long chains which drive the organization of the system.[48] While such ordered systems have many advantages, they are not necessary for this application; a more important parameter is the availability of free thiols to anchor clusters, which was optimized in the gold samples by the use of short-chain dithiols. The short chains were necessary to avoid the problems of dithiols looping on the gold surface as referred to by Bain et al.[31] These species, such as hexanedithiol, cannot bind both ends to the metal without inducing unfavorable steric interactions between the hydrogens. Contact angle measurements of 1,6-hexanedithiol on gold average between 40° and 50°, consistent with observed contact angles of free alcohols.[11] Also, the success of these samples in binding cadmium-rich clusters indicates the presence of available thiols. For the aluminum samples, thioglycolic acid was used (Figure 1B) so that the surface would be identical to that of water-soluble clusters on aluminum (Figure 1C). Such a short chain acid would lead to a quite disordered surface, but for this application the presence of free thiols close to the metal is far more important.

The clusters bound to the metal surfaces using SAMs do not charge up in photoemission experiments. This is clear from comparison of photoemission data on nanocrystals deposited by pressing into metal foils versus the SAM-bound samples. In the pressed samples, all the core level emission lines were shifted by the same amount, typically a few volts, and the widths, especially of the valence band, were increased substantially. The lack of charging in the covalently attached samples was evident. The photoemission peaks sharpened, allowing for the identification of different sulfur environments, as well as for the observation of changes in the valence band width with cluster size. The number of photoelectrons/second emitted during a typical experiment was not more than 10000, originating from an area a few square millimeters in diameter, so that the time scale for electron transfer across the SAM needs to be faster than 10 μs to avoid charging, a relatively modest requirement. We note that some other forms of electron spectroscopy, such as scanning tunneling spectroscopy, require a greater flux of charge through the sample.

Given that short chains were intentionally used to anchor the clusters, it is necessary to address how the close proximity of nanocrystals to a metal surface affects electronic spectroscopy of the clusters. Both electron- and energy-transfer rates from electronically excited molecules to metal and semiconductor surfaces drop off rapidly as a function of distance. Electron transfer drops off exponentially,[14] while dipole–dipole nonradiative energy transfer drops off with the inverse distance cubed.[49,50] At the 10-Å separation we are dealing with here, we can expect long-lived fluorescence to be nonradiatively quenched, resulting in a relative enhancement of the resonance Raman signal (Figures 17A,B) for nanocrystals bound to a metal. However, we expect the energy- and electron-transfer rates to be slow compared to the time scale of the photoemission process, so no frequency shift or broadening in the energies of the electronic states is to be expected. This conclusion is bolstered by the fact that the valence band photoemission spectra and the resonance Raman spectra from similarly sized nanocrystals are identical, regardless of whether the nanocrystals are bound to gold or aluminum, and regardless of the exact chain length employed for the SAM.

Future Work. These cluster-on-metal systems represent a new class of nanocrystal samples, well suited for many experiments. Although they were designed for application to electronic spectroscopies, resonance Raman experiments benefit from the reduced fluorescence of the sample. In addition, the metal samples are excellent thermal conductors, facilitating both low- and high-temperature studies of the nanocrystals. The first XPS studies of CdS nanocrystals provide unique information about the chemical nature of the cluster surface. Recent experiments have shown that the clusters melt at a reduced temperature,[51] and these samples are excellent candidates for the formation of thin films of bulk CdS at low temperatures.

The versatility of the synthetic technique is also an advantage. A change in the bridging group allows the distance from the metal, the type of metal, and the nature of the cluster surface species to be varied. Such direct control over these parameters is crucial for studying electron and energy transport within the nanocrystal monolayer and from the nanocrystals to the substrate. The study of interaction between nanocrystals is of great interest, since such phenomena will be very important in an ordered, organized assembly of these clusters. The images of the clusters indicate that they are packed sufficiently close together (Figure 14) and that dipole–dipole interactions between nanocrystals could influence the optical absorption spectra. If cluster size and surface preparation could be made even more uniform, it is possible that the

(48) Ulman, A.; Eilers, J. E.; Tillman, N. *Langmuir* **1989**, *5*, 1147–1152.

(49) Chance, R. R.; Prock, A.; Silbey, R. *Adv. Chem. Phys.* **1978**, *37*, 1.

(50) Waldeck, D. H.; Alivisatos, A. P.; Harris, C. B. *Surf. Sci.* **1985**, *158*, 103–125. Alivisatos, A. P.; Arndt, M. F.; Efrima, S.; Waldeck, D. H.; Harris, C. B. *J. Chem. Phys.* **1987**, *86*, 6540–6549.

(51) Goldstein, A. N.; Colvin, V. L.; Alivisatos, A. P. Observation of Melting in 30 Å Diameter CdS Nanocrystals. To appear in *Clusters and Cluster Assembled Materials*; Averback, D. S., Nelson, D. L., Bernholc, J., Eds.; Materials Research Society Symposium, Fall 1990.

nanocrystals might pack into two-dimensional arrays. Such samples would be of great interest in the study of interparticle phenomena.

Acknowledgment. This work was supported by the Director, Office of Energy Research, Office of Basic Energy Sciences, Division of Materials Sciences, of the U.S. Department of Energy, under Contract No. DE-AC03-76SF0098. V.L.C. acknowledges IBM for a predoctoral fellowship. We thank Professor Marcin Majda, Dr. C. Goss, and other members of the Majda group for their assistance in making SAMs. We thank the XPS and RBS facilities of the Lawrence Berkeley Laboratory for use of the facilities. We thank the National Center for Electron Microscopy for use of the TEMs and digitizing facilities. Finally, we thank our colleague Dr. James Tobin of Lawrence Livermore National Lab for his collaborative work on ultraviolet photoemission studies of the nanocrystals.

Registry No. Gold, 7440-57-5; aluminum, 7429-90-5; cadmium sulfide, 1306-23-6; 1,6-hexanedithiol, 1191-43-1; 2-mercaptoacetic acid, 68-11-1.

Palladium Catalysis of O_2 Reduction by Electrons Accumulated on TiO_2 Particles during Photoassisted Oxidation of Organic Compounds

Chong-Mou Wang, Adam Heller,* and Heinz Gerischer*,†

Contribution from the Department of Chemical Engineering, The University of Texas at Austin, Austin, Texas 78712-1062. *Received December 2, 1991*

Abstract: Our earlier theoretical analysis suggested that the quantum efficiency of photoassisted oxidation of organic compounds in water by O_2 on n-TiO_2 surfaces can be limited by the kinetics of the reduction of O_2. When the rate of O_2 reduction is not sufficiently fast to match the rate of reaction of holes, an excess of electrons will accumulate on the TiO_2 particles, and the rate of electron–hole recombination will increase. We now show experimentally that electrons do indeed accumulate on slurried TiO_2 particles during photoassisted oxidation of 1.6 M aqueous methanol and that electrons on the slurried particles persist for at least ~1 min even in O_2-saturated solutions. The rate of particle depolarization, i.e. of electron transfer to dissolved O_2, is increased and the negative charge on the TiO_2 particles is completely eliminated upon incorporation of Pd^0 in the surface of the TiO_2 particles. We also show that incorporation of Pd^0 in the surface increases the quantum efficiency of the photoassisted oxidation of 10^{-2} M aqueous 2,2-dichloropropionate 3-fold at 0.01 wt % Pd and 7-fold at 2 wt % Pd.

Introduction

Photoassisted oxidation of organic contaminants of water[1-15] is of interest in the context of improving the quality of water and photosolubilization of oil slicks on seawater[16] for subsequent rapid bacterial degradation.[17] Similarly, photoassisted oxidation of organic contaminants of humid air on TiO_2 is being explored. TiO_2, whether anatase or rutile, is, because of its stability and in spite of the poor overlap of its excitation spectrum and the solar spectrum, the preferred photocatalyst. The reaction catalyzed involves oxidation of surface-adsorbed water by holes to produce OH radicals that oxidize organic compounds.[18] This reaction is coupled with reduction of dissolved O_2 initially to peroxide and ultimately to water. At high concentrations of organic reagents and at high irradiance, the rate of the hole-initiated oxidation can be fast, but it cannot be faster than the rate of O_2 reduction by electrons.[19,20] When O_2 is not reduced at a sufficiently high rate, electrons accumulate on the photocatalyst and the rate of radiationless electron–hole recombination is enhanced until the sum of the rates of recombination and electron transfer to oxygen equals the rate of photogeneration of holes. In this case, the rate of photooxidation equals, and is limited by, the rate of O_2 reduction.

In our earlier theoretical analyses,[19,20] we estimated the light flux and particle size where the quantum efficiency in a TiO_2 particle slurry becomes O_2 reduction rate limited. We predicted this to be the case when the particles do not have a particularly high density of shallow, near-surface electron traps to assist in the O_2 reduction process. Whether such traps are present or not, but particularly in the absence of a high density of such traps, modification of the surface by a catalyst for O_2 reduction, for example by group VIII metals, should increase the quantum efficiency of photoassisted oxidation in photocatalyst slurries. Pt incorporation[21] in photocatalysts has been extensively studied in the past in the context of catalysis of H_2 photoproduction, but few authors considered its role in O_2 reduction in photoassisted oxidation reactions. However, Izumi et al.[1] did point out that, in the photoassisted oxidation of hydrocarbons on TiO_2 powders, the Pt cocatalyst provides a site for more efficient utilization of photogenerated electrons in the reduction of O_2. Furthermore,

† Permanent address: Fritz-Haber-Institut der Max-Planck-Gesellschaft, Faradayweg 4-6, D-W-1000, Berlin 33, Germany.

(1) Izumi, I.; Dunn, W. W.; Wilbourn, K. O.; Fan, F. R.; Bard, A. J. *J. Phys. Chem.* **1980**, *84*, 3207.
(2) Hashimoto, K.; Kawai, T.; Sakata, T. *J. Phys. Chem.* **1984**, *88*, 4083.
(3) Ollis, D. F.; Turchi, C. *Environ. Prog.* **1990**, *9*, 229.
(4) Turchi, C. S.; Ollis, D. F. *J. Catal.* **1990**, *122*, 178.
(5) Matthews, R. W. *Aust. J. Chem.* **1987**, *40*, 667.
(6) Matthews, R. W. *J. Catal.* **1988**, *111*, 264.
(7) Matthews, R. W. *Water Res.* **1990**, *24*, 653.
(8) Kormann, C.; Bahnemann, D. W.; Hoffmann, M. R. *Environ. Sci. Technol.* **1991**, *25*, 494.
(9) Al-Ekabi, H.; Serpone, N. *J. Phys. Chem.* **1988**, *92*, 5726.
(10) Pelizzetti, E.; Borgarello, M.; Minera, C.; Pramauro, E.; Borgarello, E.; Serpone, N. *Chemosphere* **1988**, *17*, 499.
(11) Barbeni, M.; Morello, M.; Pramauro, E.; Pelizzetti, E.; Vincenti, M.; Borgarello, E.; Serpone, N. *Chemosphere* **1987**, *16*, 1165.
(12) Barbeni, M.; Pramauro, E.; Pelizzetti, E.; Borgarello, E.; Serpone, N. *Chemosphere* **1985**, *14*, 195.
(13) Barbeni, M.; Pramauro, E.; Pelizzetti, E.; Borgarello, E.; Graetzel, M.; Serpone, N. *Nouv. J. Chim.* **1984**, *8*, 547.
(14) Carey, J. H.; Oliver, B. G. *Water Pollut. Res. J. Can.* **1980**, *15*, 157.
(15) Fujihira, M.; Satoh, Y.; Osa, T. *J. Electroanal. Chem. Interfacial Electrochem.* **1981**, *126*, 277.
(16) Jackson, N. B.; Wang, C. M.; Luo, Z.; Schwitzgebel, J.; Ekerdt, J. G.; Brock, J. R.; Heller, A. *J. Electrochem. Soc.* **1991**, *138*, 3660.
(17) Carey, J. H.; Oliver, B. G. *Water Pollut. Res. J. Can.* **1980**, *15*, 157.
(18) Jaeger, C. D.; Bard, A. J. *J. Phys. Chem.* **1979**, *83*, 3146.
(19) Gerischer, H.; Heller, A. *J. Phys. Chem.* **1991**, *95*, 5261.
(20) Gerischer, H.; Heller, A. *J. Electrochem. Soc.* **1992**, *139*, 113.
(21) Kraeutler, B.; Bard, A. J. *J. Am. Chem. Soc.* **1978**, *100*, 4317.

0002-7863/92/1514-5230$03.00/0